

Recurrent neural networks and transfer learning for elasto-plasticity in woven composites

E. Ghane^a, M. Fagerström^b, S.M. Mirkhalaf^{a,*}

^a*Department of Physics, University of Gothenburg, Gothenburg, Sweden*

^b*Department of Industrial and Materials Science, Chalmers University of Technology, Gothenburg, Sweden*

Abstract

As a surrogate for computationally intensive meso-scale simulation of woven composites, this article presents Recurrent Neural Network (RNN) models. Leveraging the power of transfer learning, the initialization challenges and sparse data issues inherent in cyclic shear strain loads are addressed in the RNN models. A mean-field model generates a comprehensive data set representing elasto-plastic behavior. In simulations, arbitrary six-dimensional strain histories are used to predict stresses under random walking as the source task and cyclic loading conditions as the target task. Incorporating sub-scale properties enhances RNN versatility. In order to achieve accurate predictions, the model uses a grid search method to tune network architecture and hyper-parameter configurations. The results of this study demonstrate that transfer learning can be used to effectively adapt the RNN to varying strain conditions, which establishes its potential as a useful tool for modeling path-dependent responses in woven composites.

Keywords: Textile fibres, Plastic deformation, Computational modelling, Recurrent neural networks, Transfer-learning

1. Introduction

Composite laminates consisting of woven laminae offer distinct advantages over laminates made from unidirectional laminae, particularly in terms of mechanical properties. These materials are increasingly found in structural applications due to their mechanical performance and enhanced resistance to delamination [1]. However, modeling of woven composites presents significant challenges due to the presence of two heterogeneous sub-scales, meso-scale and the micro-scale, and the intricate interlacing of yarns, resulting in the development of complex stress states [2].

In order to predict the complex behavior of woven composites governed by the heterogeneous sub-scales configuration, different full-field micro-mechanical and meso-scale models have been developed (*e.g.*, [2–4]). However, one of the major challenges

*Email: mohsen.mirkhalaf@physics.gu.se

of using meso-scale models is their high computational cost, which hinders the usage of these models for engineering applications [5]. As a remedy, mean-field models have been proposed and used (*e.g.*, [6]). In these models, average stress and average strain are considered for each sub-scale constituent. A better computational performance (compared to full-field models) is obtained.

Recently, data-driven approaches have gained considerable interest in developing surrogate models for different composites (*e.g.*, [7–12]). Different kinds of Artificial Neural Networks (ANNs) have been used to develop remarkably efficient and highly accurate surrogate models. A feed-forward architecture is typically good enough to develop an ANN-enhanced model in the linear elastic regime [13]. However, for inelastic path-dependent behavior, it is required to use more advanced ANN architectures [14]. In recent years, different kinds of Recurrent Neural Networks (RNNs), such as Gated Recurrent Units (GRU)[15] and Long Short-Term Memory (LSTM) networks [16], have been employed for the inelastic path-dependent behavior of different composite materials (see, *e.g.*, [9, 17–19]). A remarkable computational enhancement and a high level of accuracy were obtained.

Training RNNs is sensitive to initializing the training parameters (weights and thresholds) due to the risk of vanishing or exploding gradients [20]. Vanishing gradients result in slow learning, while exploding gradients lead to unstable training. Some methods have been suggested for initializing layer weights and biases [20, 21]. These methods can greatly impact how well the deep network trains. However, they are still based on randomly initializing the training parameters. Furthermore, RNNs encounter challenges when dealing with sparse feature data sets where inputs have many zero values. For instance, in the case of a stress prediction task using strain tensor components as inputs, when we have pure-shear loading, only one component of the input feature is non-zero. Data sparsity can interfere with the learning process and hinder the network’s ability to capture meaningful patterns. This paper employed a physics-guided initialization [22] of weights and thresholds using *transfer learning* [23]. Using transfer learning, RNNs are able to overcome initialization challenges by leveraging knowledge derived from previously trained models. Initially, the network is trained with an a priori model containing the expected material parameters, known as the source task. The network is then fine-tuned in accordance with the target task. In this study, the source task is intended to predict six-dimensional homogenized stress components of generic elasto-plastic constituents’ material properties of woven composites under random walk strain loadings, and the target task is to predict stresses under conventional cyclic strain loading. Models that have been trained on dense or diverse data sets can provide more robust representations of features that can be generalized well to sparse data sets. This approach accelerates training, enhances generalization over sparse feature samples, and facilitates effective learning.

This investigation has formulated various GRU and LSTM models to characterize woven composites’ elasto-plastic behavior. The specific nature of the task determines the choice between GRU and

LSTM architectures. Moreover, the optimal performance of these models is closely linked to both the number of training parameters. This facet is evaluated in depth within the framework of this study. To generate the required data set, a mean-field model from Digimat-MF [24] is employed. The matrix and reinforcements are attributed elasto-plasticity and elasticity, respectively. Notably departing from prevailing trends observed in the development of material-specific ANN surrogate models for composites (cf. [9, 25]), this study uniquely incorporates generic matrices and reinforcements into its framework.

Six-dimensional arbitrary loading paths (for six independent strain components) have been generated and applied to the sub-scale (meso-structural) simulations. The simulation results serve as a data set for the source task. Bi-axial and pure shear cyclic load paths are generated for the target task data set, each containing a different peak strain, strain ratio, load ratio, and number of cycles. As a result, two comprehensive data sets (including stress-strain responses) for generic woven composites (different matrices and reinforcements) subjected to randomly sampled and cyclic loading histories have been generated.

When training a neural network, highly sensitive parameters and hyper-parameters are present, such as learning rate, minibatch size, regularization strength, dropout rate, and network architecture [26]. The best combination of hyper-parameters requires a comprehensive study, which is frequently neglected throughout the literature due to the time-consuming nature of the process [17, 19, 27–30].

We have attempted to determine an optimal network by testing many possible combinations. The results show that an RNN model has been successfully trained and validated on the target task, enabling highly efficient elasto-plastic path-dependent simulations.

The remainder of this paper is structured as follows. Section 2 describes the data generation process, including the sub-scale mean-field modeling approach, material constituents, and design of computational experiments. Section 3 details the RNN model design and training and transfer-learning strategy. The obtained results and comparisons to micro-mechanical simulations are presented in Section 4, followed by a discussion of the developed RNN model. Concluding remarks are provided in Section 5.

2. Data generation

Every data sample contains (i) a particular set of constituent material properties, (ii) a 6D random strain loading path, and (iii) a 6D time history of homogenized stress components. The database is generated, considering various material parameters and loading conditions to capture the complex behavior of various woven composites subjected to complex strain states. Two comprehensive data sets

(one for the random walk ¹ loading and one for the cyclic loads) are created by carefully controlling the input variables and using mean-field simulations.

2.1. Meso-scale simulations

A mean-field model which uses the Mori-Tanaka theory for homogenization, implemented in DIGIMAT-MF, is used to conduct non-linear path-dependent elasto-plastic simulations of different woven composites. While the weave pattern and geometry of the meso-scale structure remain unchanged, the micro-structural constituents properties changed in each sample. As a consequence, the mean-field homogenization procedure involves a two-step process. In the first step, the sub-scale of the composite material being studied is divided into smaller units called pseudo-grains (PGs). Each PG represents a localized region within the composite. Once the division into PGs is completed, the homogenization process begins. Each pseudo-grain is individually subjected to a homogenization procedure, where the behavior and properties of the constituent materials within the PG are analyzed. In the second step, homogenization is extended to the entire sub-scale. The effective response of the entire sub-scale is computed by considering the collective behavior of all the homogenized pseudo-grains. An interested reader is referred to [31] for a more comprehensive understanding of the modeling approach.

2.1.1. Constitutive behavior of sub-scale phases

Polymeric materials typically show a strain rate dependent mechanical response (see, *e.g.*, [32, 33]). However, for most thermoset polymeric materials, under quasi-static loading rates and at room temperature, an approximation of rate-independent behavior could be considered. Therefore, in this study, a rate-independent elasto-plastic response is considered for the matrix material. The matrix is assumed to obey J_2 -plasticity with linear-exponential hardening [34]. The yield function is given by

$$\Phi(\sigma, \kappa) = \sigma_{\text{eq}} - (\sigma_y + \kappa) \leq 0, \quad (1)$$

where σ_y is the yield stress, and σ_{eq} is the von Mises equivalent stress defined by

$$\sigma_{\text{eq}} = \sqrt{\frac{3}{2} \boldsymbol{\sigma}_{\text{dev}} : \boldsymbol{\sigma}_{\text{dev}}}, \quad \boldsymbol{\sigma}_{\text{dev}} = \boldsymbol{\sigma} - \frac{1}{3} \text{tr}(\boldsymbol{\sigma}) \mathbf{I}. \quad (2)$$

In Equation (2), $\boldsymbol{\sigma}_{\text{dev}}$ is the deviatoric stress tensor, and \mathbf{I} is the second-order identity tensor. In Equation (1), k is the hardening stress which is given by

$$\kappa = H \bar{\epsilon}^p + H_\infty \left(1 - e^{-m \bar{\epsilon}^p} \right), \quad (3)$$

¹It's worth noting that the term "random walk" is often associated with stochastic processes, where an unpredictable element determine the next step or state. Random walks in strain loading suggest that a strain value evolves over time as a result of random factors, resulting in a pattern that may resemble a walker's path.

where H is the linear hardening modulus, H_∞ is referred to as the hardening modulus, $m > 0$ is the hardening exponent, and $\bar{\varepsilon}^P \geq 0$ is the accumulated plastic strain.

Reinforcements are assumed to be isotropic and linearly elastic and obey Hooke’s generalized law. Furthermore, it is assumed that the matrix and reinforcement phases are perfectly bonded. Despite the fact that this assumption may not be true in all cases, it provides a reasonable basis for examining the overall behavior of the woven composite under study.

2.2. Design of computational experiments

This study involves two sets of input features for computational experiments: (i) static features representing fiber and matrix material properties, and (ii) multi-dimensional sequential load path components (Section 2.2.2). A wide range of properties are considered for the static features, which are given in Table 1.

Table 1: Ranges of material parameters used to generate the required data set during simulations. All data samples in the training and testing sets are distinguished by a unique set of properties of their micro-structural constituents.

	Parameter	Value
Fiber	Young’s modulus E_F	69-700 GPa
	Poisson’s ratio ν_F	0.25-0.49
	Fiber volume fraction V_f	0.10 – 0.48
Matrix	Young’s modulus E_M	2-10 GPa
	Poisson’s ratio ν_M	0.2-0.49
	Yield stress σ_y	31-66 MPa
	Linear hardening modulus H	1-200 MPa
	Hardening modulus H_∞	10-30 MPa
	Hardening exponent m	1-500

2.2.1. Sampling material features

To properly train an ANN, it is beneficial to have uniformly distributed input features. Regular grids of sample points can lead to coincident projections in different hyper-planes [11], negatively impacting machine learning, especially in high-dimensional spaces [35]. To obtain a good correlation between regular grids and random distributions, it is necessary to have consistent data sets. Thus, using an effective sampling technique helps to achieve a random and uniform distribution while reducing simulation costs.

Random sampling and stratified sampling often result in clusters and gaps in a data set. Alternatively, Sobol sequence sampling [36], a quasi-random sampling technique, offers a solution. Unlike other pseudo-random algorithms, Sobol sequence sampling avoids clustering and gaps even in smaller data

sets [37]. It aims to generate multiple parameters uniformly distributed across a multi-dimensional parameter space.

Thus, in the current work, Sobol sequence sampling is employed to generate a comprehensive design space. More than 10,000 data samples are generated with different combinations of the static features given in Table 1. The resulting design space enables the exploration of various material and micro-structural configurations, providing valuable insights into the behavior of woven composite materials.

For visualizing high-dimensional data sets, t-SNE (t-Distributed Stochastic Neighbor Embedding) is utilized [38, 39]. It minimizes the discrepancy between high-dimensional and low-dimensional distributions using the Kullback-Leibler (KL) divergence [40] as a cost function. KL divergence quantifies how one probability distribution (from a multi-dimensional space) diverges from the expected (into a 2D space) probability distribution. The algorithm iteratively adjusts data point positions to minimize the cost function. Monitoring KL divergence during cost minimization indicates capturing data structure successfully and relationships in the lower-dimensional domain. t-SNE preserves local structures, patterns, and clusters. While it is primarily a visualization tool, it can effectively represent data distribution, as shown in Figure 1. No pattern or gap is visible on the scattered 2D plot, indicating a

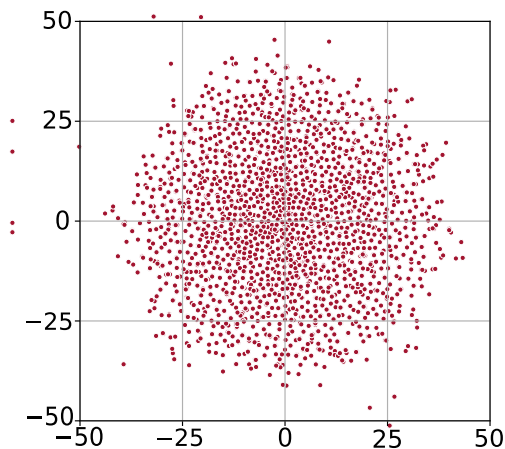


Figure 1: t-SNE distribution of 9 dimensional static feature space described in Table 1. Different micro-structural configurations are described by 3 fiber elasticity, 3 matrix elasticity and 3 matrix plasticity feature parameters.

good correlation between regular grids and random distributions in the static feature space.

2.2.2. Loading path generator

In order to sample representative strain paths, different approaches can be employed, *e.g.*, [19, 41]. In the source task, a random walk, representing long-term trends, is combined with noises, representing local variations. The algorithm [19] utilizes a six-dimensional space for independent strain components.

Components are sampled independently from a normal distribution to generate direction vectors, which are then normalized to unit vectors. The algorithm defines parameters: N as the total number of steps, n_1 as the number of drift directions (the number of major changes in the loading direction), n_2 as the steps per drift direction (noises), and γ as the perturbation amplitude factor. Assuming equal n_1 and n_2 , a time series is created by combining a number of drift directions and perturbation vectors. Figure 2 shows four samples of the generated loading paths.

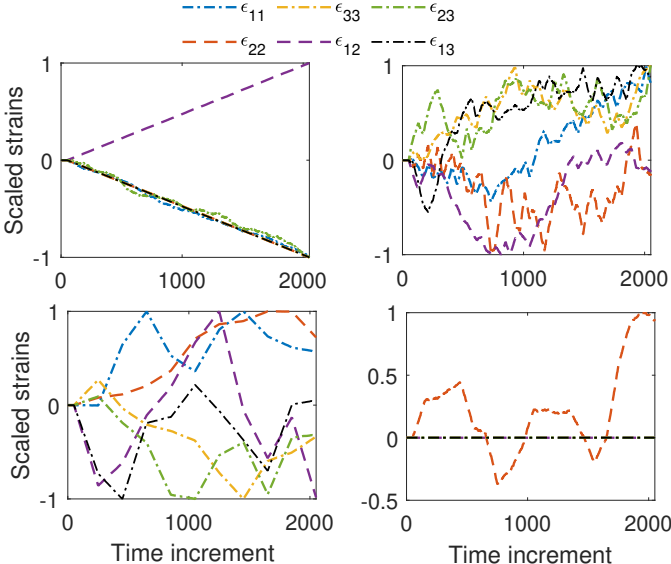


Figure 2: Four samples of input strain loading paths from random walk data set (scaled between [-1,1]). Each graph contains six components of the strain tensor applied on a randomly chosen material set.

Some of the loading samples have sparsity in their input features, such as the fourth case in Figure 2, where the input strain tensor only includes the transverse strain component, while all other components are zero. Since this rarely occurs, the trained network based on such a data set may not be able to generalize the solution to cases with high feature sparsity, such as conventional cyclic loadings. Therefore, the second data set is generated based only on cyclic loads in shear and bi-axial load cases where plasticity is significant in woven composites. Figure 3 shows four samples from the second data set. Indicating factors in the cyclic loads include the peak strain value, the strain ratio (ratio of shear strain to tensile strain in bi-axial scenarios), the load ratio (fraction of the maximum positive strain to the minimum negative strain value), and the number of cycles.

3. Recurrent neural networks

RNNs excel in handling sequences of long lengths, making them suitable for language modeling, speech recognition [42], machine translation [15, 43], and time-series prediction [40]. RNNs effectively model sequential data due to their internal memory, capturing temporal dependencies. Feedback loops

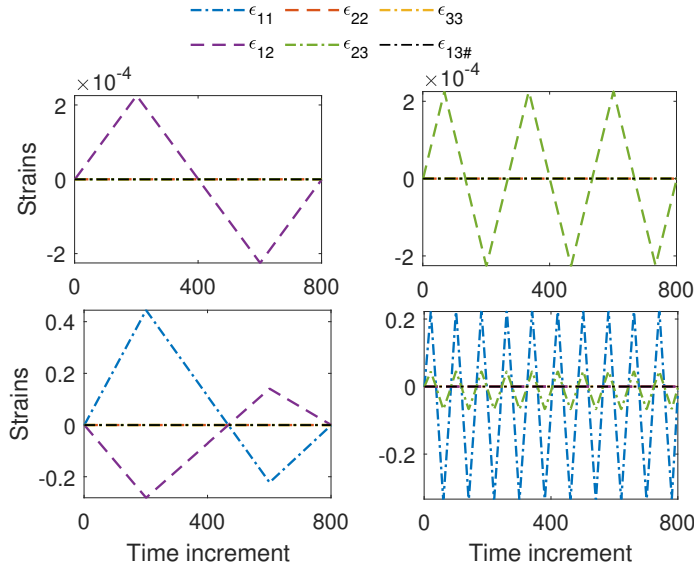


Figure 3: Four samples of input strain loading paths from a smooth cyclic path data set. Each graph contains six components of the strain tensor applied on a randomly chosen material set. The smooth cyclic loading paths include (from up-left to down-right) pure in-plane shear ϵ_{12} , out-of-plane shear ϵ_{23} and bi-axial $[\epsilon_{11}, \epsilon_{12}]$ and $[\epsilon_{12}, \epsilon_{23}]$ loading.

in the RNN architecture enable information flow between input and output, maintaining an internal state for predictions based on current and past inputs.

3.1. Transfer learning rescues RNNs from initialization and sparsity hurdles

In the paradigm of transfer learning, a model initially trained on a source task with abundant data serves as a foundational framework for a closely related target task. The primary objective is to leverage the pre-trained model’s acquired knowledge of features, representations, and patterns to enhance the learning process on the target task [23]. Furthermore, during the training phase for the source task, pre-trained models undergo regularization mechanisms, which mitigate overfitting risks and augment generalization capabilities when subsequently fine-tuned for the target task. Transfer learning entails initializing the model with optimized weights specific to certain features, resulting in noteworthy acceleration of convergence and optimization improvements tailored for the target task. Transfer learning has been proven to be useful for data fusion in elastic regime [44] and elasto-plastic behavior of short-fiber composites [45].

One specific strategy within transfer learning is fine-tuning [41]. This approach is employed when the source and target tasks exhibit close relatedness, allowing for the adjustment of weights in a pre-trained model based on the data specific to the target task. In the context of this study, the source task involves predicting the six components of stress sequences derived from random loading simulations. Subsequently, during the original network training, the target task is formulated to predict stress components associated with cyclic loading paths. The RNN model employed for the

source task integrates an a priori model, initially trained on extensive data sets, to adapt and enhance its performance on novel tasks. The weights and biases derived from the neural networks at the end of training serve as the initialization for the neural networks used in transfer learning.

3.2. Recurrent learning with GRU and LSTM units

Gated Recurrent Units (GRUs) and Long Short-Term Memory (LSTM) networks are two types of recurrent neural networks (RNNs) that address the vanishing and exploding gradient problems encountered in traditional RNNs [26, 46, 47]. GRUs use two so-called gating mechanisms, an update gate and a reset gate, to selectively update and reset their hidden state. This enables them to gather information across time steps and retain long-term dependencies [48]. LSTM units, on the other hand, employ three gating mechanisms: the input gate, the forget gate, and the output gate. These gate mechanisms control the flow of information, select information to retain or discard, and filter relevant information for output, respectively [16]. An interested reader is referred to [49] for a more comprehensive understanding of LSTM and GRU units.

Since GRUs have only two gates, they are computationally more efficient and easier to train with fewer parameters. However, they may not be as effective at capturing complex long-term dependencies as LSTMs. LSTMs with three gating mechanisms can model more complex relationships over longer sequences, but they have a greater computational cost and require more training data to prevent overfitting [50]. The choice between GRUs and LSTMs depends on the specific task at hand, the availability of computational resources, and the desired trade-off between model complexity and performance. To better understand how data flows through an RNN network containing two layers of recurrent units, Figure 4 is provided.

3.3. Feature scaling

Differences in input variable magnitudes can bias neural networks and hinder network learning. Variables with larger values dominate and overshadow smaller ones, leading to unstable weight updates and sub-optimal performance. Standardization equalizes input feature scales, ensuring smoother convergence in the network training and preventing disproportionate variable influence. It also allows direct magnitude comparison and enhances interpretability, thereby promoting stable training, faster convergence, and improved neural network performance [40].

The standardization process involves normalizing sequential strain components to an absolute maximum value of one. Non-sequential material properties undergo min-max scaling to have values between zero and one. This enables neural networks to capture the underlying patterns better, resulting in an improved performance and reliable predictions.

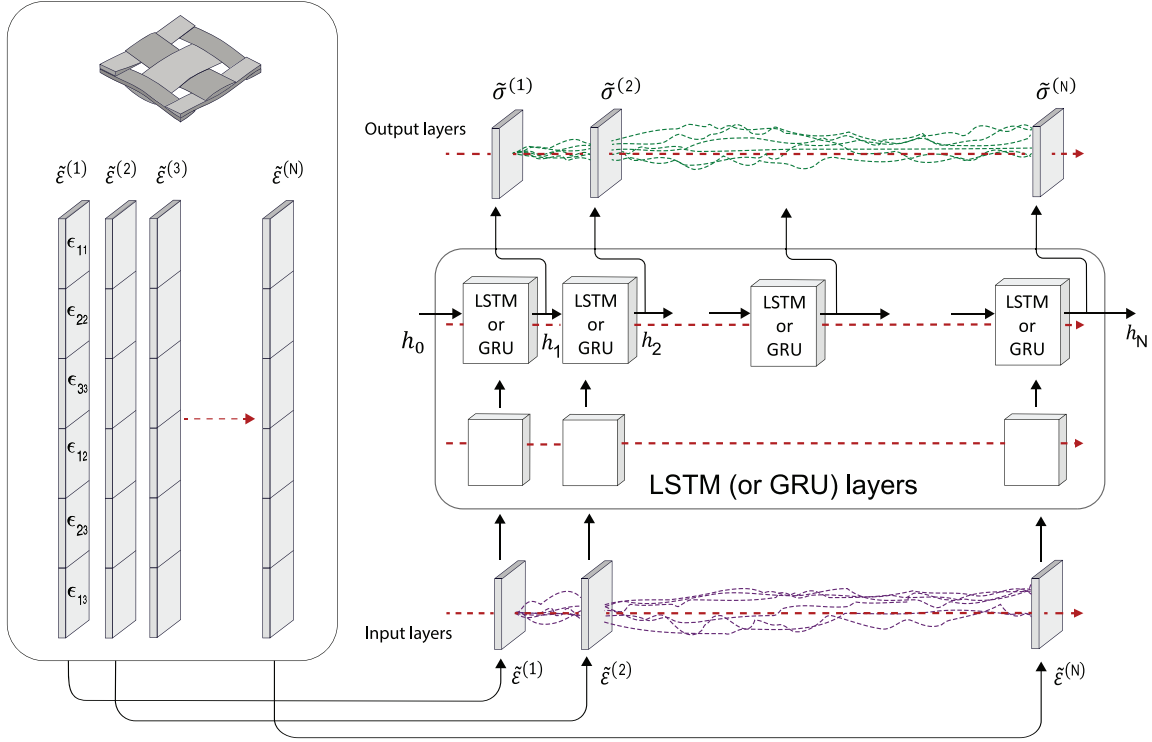


Figure 4: A schematic representation of the data flow for feeding the RNN model with a data sample. As shown on the left side of the figure, a woven composite and strain loading paths have been randomly sampled from the data set. Each stripe represents a time step of the strain tensor ($\tilde{\epsilon}^{(t)}$) containing six strain components ($\epsilon_{i,j}$). Red dashed lines indicate time increments in a load path. Six random loads are presented in the input layer in purple. Afterwards, the data propagates through the LSTM (or GRU) network layers. The network outputs are in green. The internal variables flow can also be seen in one of the network layers. A hidden (and/or cell) state is indicated by h_t .

3.4. Metrics beyond loss

Network performance relies not only on architecture but also on hyper-parameters like learning rate, regularization strength, batch size, etc. The choice of hyper-parameters can significantly impact the validation loss, potentially overshadowing the effect of selecting the optimal network architecture based solely on validation loss.

This study considers additional evaluation metrics to find an optimal network configuration. To represent all output stress components, the von Mises stress definition is adopted:

$$\sigma_{\text{vM}} = \sqrt{\frac{1}{2} \left[(\sigma_{11} - \sigma_{22})^2 + (\sigma_{22} - \sigma_{33})^2 + (\sigma_{33} - \sigma_{11})^2 + 6(\sigma_{12}^2 + \sigma_{23}^2 + \sigma_{31}^2) \right]}. \quad (4)$$

Using the von Mises effective stress, a single sequential vector is computed based on the six individual sequences of stress components (σ_{ij} and $i, j = 1, 2, 3$).

Three statistical measures [51] are used to assess and compare the predictive performance of multiple

neural network configurations. In the following, $e_i^{(t)}$ represents an individual model-prediction error at time step t , defined as

$$e_i^{(t)} = \sigma_{vM}^{(t)} - \hat{\sigma}_{vM}^{(t)}, \quad (5)$$

where $\hat{\sigma}_{vM}^{(t)}$ is the predicted equivalent stress at time step t and $\sigma_{vM}^{(t)}$ is the true equivalent stress at t .

Mean Absolute Error

The mean Absolute Error (MAE) measures the average magnitude of errors between the predicted and desired values. MAE is calculated by taking the average of the absolute differences between each predicted and desired value, normalized by the number tested samples from the unseen data set (n):

$$\text{MAE} = \frac{1}{n} \sum_{t=1}^n |e_i^{(t)}|. \quad (6)$$

MAE provides an indication of the average size of errors produced by the model. There is no consideration for the direction of errors (overestimation or underestimation), and all errors are given equal weight. A lower MAE indicates a better performance.

Root Mean Square Error

Another commonly used measure of prediction error is the Root Mean Square Error (RMSE). It is obtained by taking the square root of the average of the squared differences between the predicted values and the desired values as

$$\text{RMSE} = \sqrt{\frac{1}{n} \sum_{t=1}^n (e_i^{(t)})^2}. \quad (7)$$

Due to the squaring operation, larger errors are penalized more heavily. RMSE gives a measure of the overall deviation or dispersion of errors. Similarly to MAE, a lower RMSE indicates a better performance. Similarly to MAE, RMSE does not consider whether the model overestimates or underestimates a quantity at a given time instant.

Mean Bias Error

The bias or Mean Bias Error (MBE) refers to the systematic deviation between model predictions and the desired values in a data set. Bias can be positive or negative, indicating whether the predictions consistently overestimate or underestimate desired values. The scale and units of the predicted and desired values typically determine the bias range. MBE is computed by

$$\text{MBE} = \frac{1}{n} \sum_{t=1}^n e_i^{(t)}. \quad (8)$$

4. Results and discussion

To account for path-dependent plasticity, we utilize GRU and LSTM, improved versions of standard recurrent neural networks that can effectively model sequential data. The network input consists of sequential data with 15 different features, concatenating 6 sequential strain tensor components and 9 static material properties. In each instance, the non-sequential features (the material properties) are repeated throughout the entire sequence of $N_T = 2000$ pseudo-time increments. For data consistency, only completed simulations are used¹. The output signals are components of the stress tensor. The mean squared error loss function is computed at the regression layer and is given by

$$L = \frac{1}{N_{\text{batch}}} \sum_{k=1}^{N_{\text{batch}}} L_k, \quad \text{with} \quad L_k = \frac{1}{2N_T} \sum_{i=1}^F \sum_{j=1}^{N_T} (\hat{y}_{ij}^k - y_{ij}^k)^2, \quad (9)$$

where \hat{y}_{ij}^k and y_{ij}^k are the k^{th} predictions and target values in a training batch, respectively, F is the number of output features, N_T is the data sequence length, and N_{batch} is the batch size. The computational programming language MATLAB [49] is employed for implementing recurrent neural networks. Training for different network configurations is done on the Vera hardware [52] at Chalmers University of Technology.

Two data sets are generated, including 28,000 data samples for the source task on random walk loading paths, and 10,000 samples for the target task on smooth cyclic loading paths. Each data set is randomly split into training (80%), validation (10%), and test (10%) sets. For each task, the training data set is iteratively passed through the neural network for multiple epochs, with shuffled data at each epoch. The validation set helps for tuning hyper-parameters, such as batch size, learning rate, and regularization parameters, to achieve an optimal model performance. The test set serves as unseen data for final performance evaluation after the network training and validation.

Section 4.1 presents results related to the source task. The purpose of Section 4.2 is to emphasize the importance of tuning the network architecture and hyper-parameters. Once the network’s generalization ability is confirmed for a random load path, the transfer learning method is used in Section 4.3 for training a network to predict smooth cyclic loads (target task).

4.1. Prediction on the random strains test samples

A piece-wise learning rate decay strategy is employed, reducing the learning rate by 10% every ten epochs to enhance convergence. The training process uses ADAM optimizer [53]. In order to prevent overfitting, early stopping is used instead of a fixed number of epochs. Training stops when the model’s performance on the validation set plateaus while the loss on the training set continues to decrease.

¹Some of the simulations with the highest number of loading drifts (200) are not converged in the Digimat-MF solver.

Figure 5 illustrates the loss evolution for LSTM and GRU networks in accordance with Equation 9. The plateau region on the validation set indicates convergence in the training of both cases. While the GRU network struggles more to reach the minimum loss value at the beginning, the minimum loss values are almost equal.

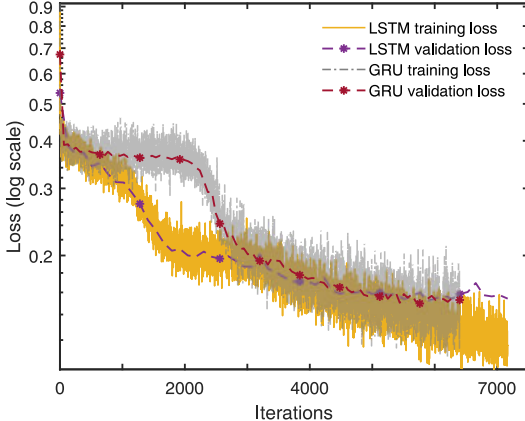
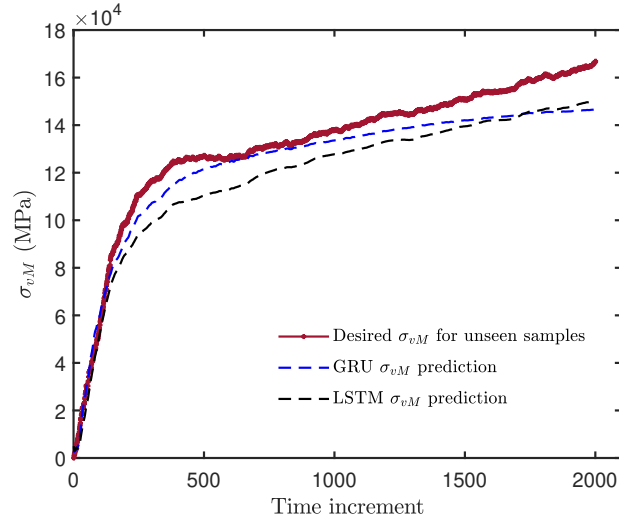


Figure 5: Two examples of the training and validation loss evolutions on the random strain data set. Each network consists of three layers with 512 units of LSTM or GRU plus a 50% dropout after the first layer. In both cases, the learning rate is 0.001, the L_2 regularization is set to 0.001, and the minibatch size is 128. Yellow and gray lines indicate the training loss calculated at each iteration. The dashed lines in red and purple indicate the loss calculated at the end of each epoch for the validation set.

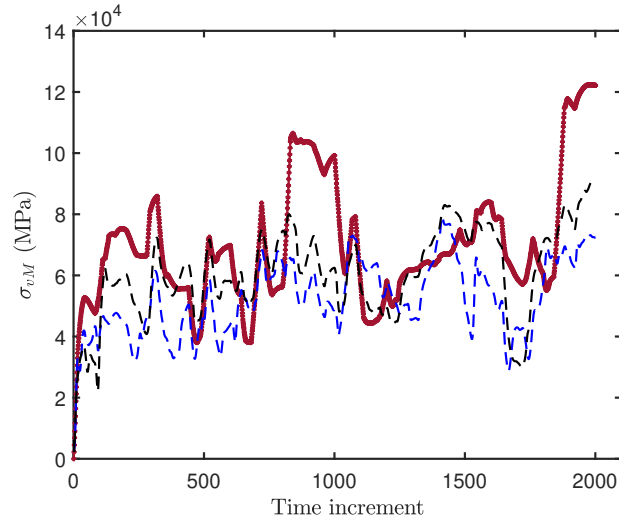
The three metrics, defined in Section 3.4, are computed based on the predictions made for each sample in the test set. This results in three sequences of length N_T of error metrics. First, we determine the average MAE, MBE, and RMSE for all test samples through the pseudo-time steps. Afterward, the mean value over pseudo-time steps for three error matrices is obtained and presented in Tables 1 and 2 in supplementary materials for different network architectures and the number of training parameters. To find the best architecture, these tables show the performance characteristics of different GRU and LSTM network configurations. The dropout rate is abbreviated as "dp," and the minimum values in each column are given in bold numbers. For detailed error evaluations on GRU and LSTM networks, the reader is referred to the supplementary material of this study. Our objective is to determine the optimal architecture first; afterward, various hyper-parameters are discussed using LSTM or GRU units in Section 4.2. Based on von Mises stress, Figure 6 compares the performance of two LSTM and GRU networks in predicting two random walk loads from the unseen data set.

The network configuration is defined by the number of GRU (or LSTM) units and the specification of the subsequent dropout layer. For example, the "3GRU(128) dp(40%)" network consists of three GRU layers, each containing 128 units, followed by a 40% dropout layer.

Although the smallest network "GRU(32)" had the lowest validation loss, it can not generalize well



(a)



(b)

Figure 6: Candidate LSTM (dashed black lines) and GRU (dashed blue lines) predictions on two samples with (a) $n_1 = 3$ and (b) 15 drift directions from the random walk paths of the unseen data set. von Mises stress is plotted in real scale.

due to higher MAE and RMSE error ranges when testing unseen test data. "3LSTM(512) dp(50%)" displayed the lowest MAE and RMSE, indicating better prediction and generalization on unseen data than other models. However, note that the MBE of "3LSTM(512) dp(50%)" is not closest to zero, suggesting a potential underestimation of equivalent stress.

In figure 7, "3LSTM(512) dp(50%)" predictions are shown for stress components on two randomly selected test samples. Figure 7a shows a strong correlation between the predictions and the desired

stress values. However, stress prediction deviates for σ_{33} , where the desired value is close to zero throughout the loading increments. It is potentially related to the general underlying issue with neural networks, known as feature sparsity [40], which needs further research to handle sequential regression tasks. It is possible that a network might have difficulty predicting features that are close to zero in a sample when there is a high number of input features (15 in this case).

In spite of a highly random loading path, in 7b, the predicted values match well with the desired values from mean-field simulation. It can be seen that the predictions on normal components are better than those on shear components. This observation can be attributed to woven composites’ physical behavior, where normal stress components predominantly influence the overall response. The shear components are of a much lower order of magnitude, resulting in relatively more minor effects in the training of the network.

4.2. Discussion on hyper-parameters

Learning rate, minibatch size, regularization strength, dropout rate, and network architecture are crucial parameters during an RNN training. This is especially critical before the transfer learning process on the target task. Regularization (also called weight decay) [35] adds a penalty term to the loss function, promoting smaller weights in the network. This prevents the model from becoming overly sensitive to training data and enhances its ability to generalize to unseen data. Additionally, the dropout layer [54] randomly sets a fraction of input units to zero during training, preventing co-adaptation of neurons and encouraging the network to learn more robust and independent representations. Combining L_2 regularization with dropout mitigates overfitting, reduces model complexity, and fosters more generalizable representations [55]. Gradient clipping, setting the absolute value to one or using the maximum of normalized features, helps eliminate exploding gradients [26].

Various networks have undergone grid search training to find the best hyper-parameter combination. The tested hyper-parameters have been examined as follows: Minibatch Size = [16, 32, 64, 128], L_2 Regularization = [0.001, 0.01, 0.], Dropout Rate = [0.2, 0.5, 0.8], Learning Rate = [0.0001, 0.001, 0.01]. The grid search method leads to training and evaluating more than 200 LSTM and GRU networks with different hyper-parameter combinations.

For detailed error evaluations, please refer to Table 3 in the supplementary material of this study.

Figure 8 presents the results of hyper-parameter tuning for candidate LSTM and GRU networks from Section 4.1, featuring three layers with 512 units each. The figure highlights the best hyper-parameter combination for optimal performance. The LSTM network’s optimum learning rate and minibatch size are 0.001 and 128, respectively, while the candidate GRU network optimum is 0.1 and 32. The regularization and the dropout rate are optimal in both networks at 0.001 and 50%, respectively. While LSTM networks outperform GRU networks in minimizing RMSE and MAE, they

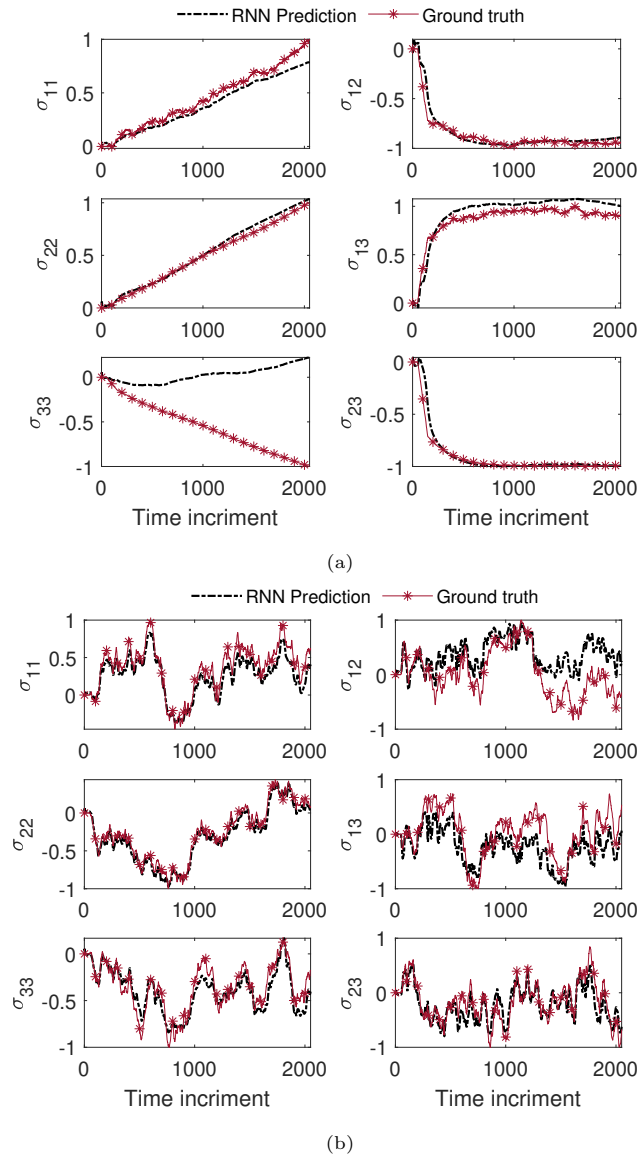


Figure 7: Network (3LSTM(512) dp(50%)) predictions against micro-mechanical results for two samples from unseen random load cases. Stress values are scaled between $[-1, 1]$ (a) Six components of stresses in a case with a rather uniform load and (b) a case with high randomness in loading. The solid red line is the mean-field simulation output (desired values), and the dashed black lines are the network predictions.

come with the cost of, on average, 15 times longer training times.

4.3. Prediction on conventional load cycles

The initial task, referred to as the source task, involves predicting loading cases associated with random walk loading paths. Subsequently, the focus shifts to the target task, wherein the objective is

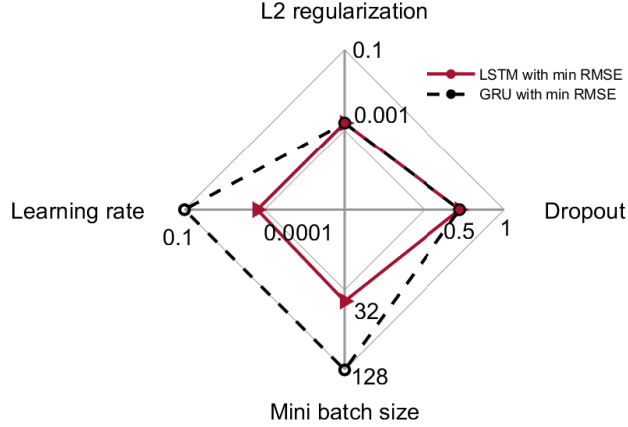


Figure 8: Hyper-parameter combinations for the candidate LSTM and GRU networks with three layers, each containing 512 units. The spider plot represents the examined range of four hyperparameters as represented by four axes. The red solid line indicates the optimum LSTM network and the dashed black line is the optimum GRU network. Detailed evaluations of more than 200 examined networks are presented in the supplementary material.

to predict loading paths characterized by conventional cyclic patterns.

However, a notable challenge is associated with applying the trained network to the target task involving cyclic loads. Therefore, the network undergoes fine-tuning with a data set specific to the target task. As can be seen in Figure 9, the evolution of loss illustrates the convergence of the transfer learning process following the initial training of the LSTM network.

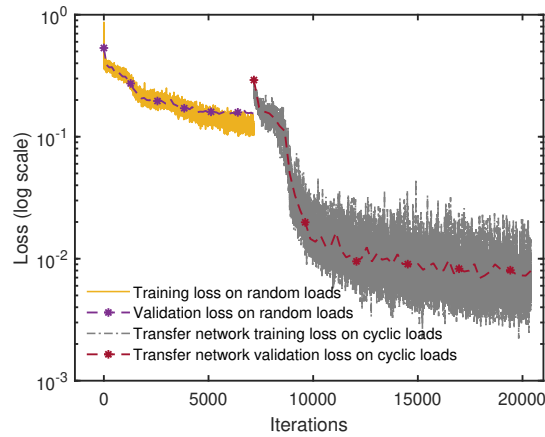


Figure 9: On the source task, the original LSTM network training and validation losses are presented in yellow and dashed purple, respectively. Transfer learning is then applied to the target task (cyclic loads), and the loss is computed (gray for training and red for validation).

There are two possible alternative scenarios: (1) the original network is limited to being trained on cyclic loads, or (2) the original network is initially trained on cyclic loads and fine-tuned with random

walk paths. Three instances of cyclic loads are shown in Figure 10, corresponding to a one-cycle test, a three-cycle test, and a ten-cycle test, respectively. It can be clearly seen that the original network

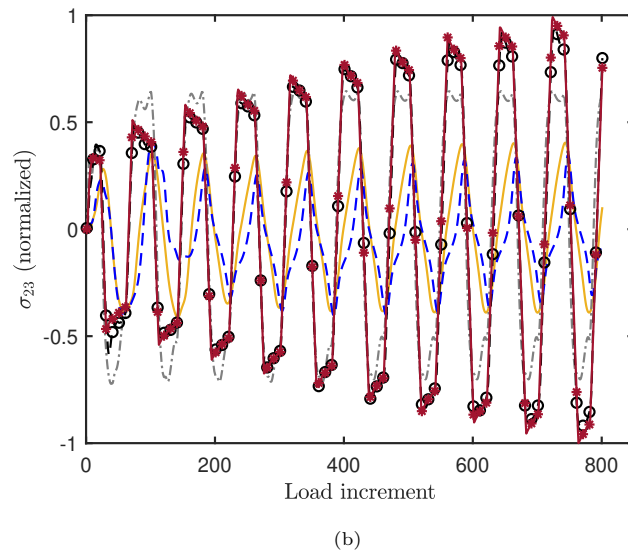
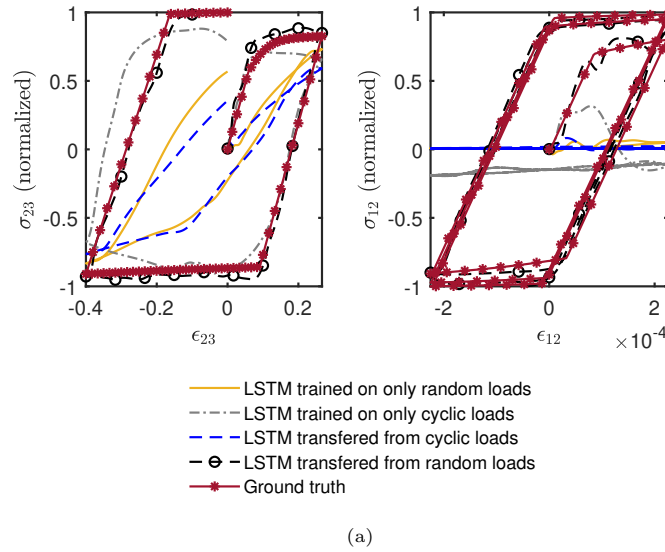


Figure 10: LSTM network predictions on conventional cyclic loading compared with desired stress values (red solid lines with stars). Stress values are normalized between $[-1, 1]$. Black dashed lines indicate the candidate transferred model predictions. The blue dashed lines indicate predictions of a model trained initially on cyclic loads and then fine-tuned by random loads. The yellow and grey lines show the predictions of models that have been trained only on random and cyclic loads, respectively. (a-left) one cycle pure out-of-plane shear, (a-right) three cycles pure in-plane shear. (b) ten cycles pure out-of-plane shear vs. load increments.

trained based on the random walk data set (represented by the solid yellow line) can not predict the cyclic loads despite its performance on the random walk data set. The dashed grey line indicates that the data set for the cyclic load is insufficient and that most of the features are too sparse to train a network to predict unseen test targets. This dashed blue line illustrates an alternative approach that involves training the network on cyclic loads and fine-tuning it using random walks. According to the results, transfer learning, in this case, cannot perform versatility.

The most promising results are obtained by training the model on random walk load paths (Section 4.1) and then fine-tuning it for cyclic loads, as illustrated by the dashed black line. With the transferred network, stress values can be predicted from sparse feature samples through the entire loading increments not only for one-cycle tests (Figure 10a-left) but also for multiple cycles (Figure 10a-right and 10b). In some cases, the predictions deviate from the desired values at the beginning of loading, as shown in Figure 10a-right. This behavior can be attributed to the nature of RNNs, which forget about the first part of a sequence when asked to predict the whole sequence at once, and not for forecasting and predicting one step ahead [50]. A comprehensive study of the dynamics of transfer learning between random walk and cyclic loading scenarios provides valuable insight into optimizing neural network performance across a wide range of application scenarios.

5. Conclusions

In conclusion, this study has investigated the capabilities of Recurrent Neural Networks (RNNs) combined with the transfer learning strategy in supervised learning of the nonlinear behavior of woven composites, specifically when plasticity is present in the matrix phase. The research has examined the predictive capacity of RNNs based on mean-field simulated data, using six independent random components of meso-scale 3D strain tensor and nine material properties as inputs and predicting six components of homogenized stresses as outputs.

Sobol sequence sampling has been employed to create a uniform and random design spaces for elastic fiber and elasto-plastic matrices with varying volume fractions. A random load sampling strategy has also ensured a diverse and comprehensive design space. Various Gated Recurrent Unit (GRU) and Long Short-Term Memory (LSTM) architectures, along with different hyper-parameters, have been explored to identify the most suitable model for predicting stresses in unseen test samples derived from random loads (source task). Subsequently, the trained network, initially exposed to random loads through transfer learning, has demonstrated satisfactory performance in predicting stress components when subjected to conventional cyclic load samples (target task). Transfer learning has demonstrated in this paper as an effective method of domain adaptation across a variety of loading types in material science datasets. This study not only creates a precedent for future investigations into transferring knowledge

across datasets of varying quality, but it also provides the necessary foundation for tailoring models for full field simulations and even scarce experimental data in future studies based on insights gained from mean field simulations.

Acknowledgment

S.M. Mirkhalaf and E. Ghane gratefully acknowledge financial support from the Swedish Research Council (VR grant: 2019-04715) and the University of Gothenburg. M. Fagerström is thankful for the support through Vinnova’s strategic innovation programme LIGHTer, in particular via the project LIGHTer Academy Phase 3 (grant no. 2020-04526). The computations were enabled by resources provided by Chalmers e-Commons at Chalmers. E. Ghane is also grateful to Joel Magnusson, Iuri Rocha and Hon Lam Cheung for their input and stimulating discussions, which enhanced this research.

References

- [1] Z. Ullah, X.-Y. Zhou, L. Kaczmarczyk, E. Archer, A. McIlhagger, and E. Harkin-Jones. A unified framework for the multi-scale computational homogenisation of 3d-textile composites. *Composites Part B: Engineering*, 167:582 – 598, 2019.
- [2] Aurélien Doitrand, Christian Fagiano, François Hild, Vincent Chiaruttini, Anne Mavel, and Martin Hirsekorn. Mesoscale analysis of damage growth in woven composites. *Composites Part A: Applied Science and Manufacturing*, 96:77–88, 2017.
- [3] Dayou Ma, Marco Giglio, and Andrea Manes. Analysis of mesoscale modelling strategies for woven composites. *Material Design & Processing Communications*, 3(3):e145, 2021.
- [4] Aurélien Doitrand, Christian Fagiano, F-X Irisarri, and Martin Hirsekorn. Comparison between voxel and consistent meso-scale models of woven composites. *Composites Part A: Applied Science and Manufacturing*, 73:143–154, 2015.
- [5] Kevin Spilker, Van-Dung Nguyen, Ling Wu, and Ludovic Noels. Three-scale bridging for woven composites using homogenization techniques. *European Journal of Mechanics-A/Solids*, 100:104974, 2023.
- [6] Ling Wu, Tianyu Zhang, Etienne Maillard, Laurent Adam, Philippe Martiny, and Ludovic Noels. Per-phase spatial correlated damage models of ud fibre reinforced composites using mean-field homogenisation; applications to notched laminate failure and yarn failure of plain woven composites. *Computers & Structures*, 257:106650, 2021.

- [7] IBCM Rocha, Pierre Kerfriden, and FP van Der Meer. On-the-fly construction of surrogate constitutive models for concurrent multiscale mechanical analysis through probabilistic machine learning. *Journal of Computational Physics: X*, 9:100083, 2021.
- [8] N. Mentges, B. Dashtbozorg, and S.M. Mirkhalaf. A micromechanics-based artificial neural networks model for elastic properties of short fiber composites. *Composites Part B: Engineering*, 213:108736, 2021.
- [9] MA Maia, IBCM Rocha, P Kerfriden, and FP van der Meer. Physically recurrent neural networks for path-dependent heterogeneous materials: Embedding constitutive models in a data-driven surrogate. *Computer Methods in Applied Mechanics and Engineering*, 407:115934, 2023.
- [10] Bassam El Said. Predicting the non-linear response of composite materials using deep recurrent convolutional neural networks. *International Journal of Solids and Structures*, 276:112334, 2023.
- [11] M. A. Bessa, R. Bostanabad, Z. Liu, A. Hu, Daniel W. Apley, C. Brinson, W. Chen, and Wing Kam Liu. A framework for data-driven analysis of materials under uncertainty: Countering the curse of dimensionality. *Computer Methods in Applied Mechanics and Engineering*, 320:633–667, 2017.
- [12] Aleksandr Dekhovich, O Taylan Turan, Jiaxiang Yi, and Miguel A Bessa. Cooperative data-driven modeling. *Computer Methods in Applied Mechanics and Engineering*, 417:116432, 2023.
- [13] E Ghane, M Fagerström, and SM Mirkhalaf. A multiscale deep learning model for elastic properties of woven composites. *International Journal of Solids and Structures*, 282:112452, 2023.
- [14] Max Rosenkranz, Karl A Kalina, Jörg Brummund, and Markus Kästner. A comparative study on different neural network architectures to model inelasticity. *arXiv preprint arXiv:2303.03402*, 2023.
- [15] Kyunghyun Cho, Bart Van Merriënboer, Caglar Gulcehre, Dzmitry Bahdanau, Fethi Bougares, Holger Schwenk, and Yoshua Bengio. Learning phrase representations using rnn encoder-decoder for statistical machine translation. *arXiv preprint arXiv:1406.1078*, 2014.
- [16] Sepp Hochreiter and Jürgen Schmidhuber. Long short-term memory. *Neural computation*, 9(8):1735–1780, 1997.
- [17] M. Mozaffar, R. Bostanabad, W. Chen, K. Ehmann, J. Cao, and M. A. Bessa. Deep learning predicts path-dependent plasticity. *Proceedings of the National Academy of Sciences*, 116(52):26414–26420, December 2019.

- [18] Ling Wu and Ludovic Noels. Recurrent neural networks (rnns) with dimensionality reduction and break down in computational mechanics; application to multi-scale localization step. *Computer Methods in Applied Mechanics and Engineering*, 390:114476, 2022.
- [19] J Friemann, B Dashtbozorg, M Fagerström, and SM Mirkhalaf. A micromechanics-based recurrent neural networks model for path-dependent cyclic deformation of short fiber composites. *International Journal for Numerical Methods in Engineering*, 124(10):2292–2314, 2023.
- [20] Xavier Glorot and Yoshua Bengio. Understanding the difficulty of training deep feedforward neural networks. In *Proceedings of the thirteenth international conference on artificial intelligence and statistics*, pages 249–256. JMLR Workshop and Conference Proceedings, 2010.
- [21] Kaiming He, Xiangyu Zhang, Shaoqing Ren, and Jian Sun. Delving deep into rectifiers: Surpassing human-level performance on imagenet classification. In *Proceedings of the IEEE international conference on computer vision*, pages 1026–1034, 2015.
- [22] Antoine Benady, Emmanuel Baranger, and Ludovic Chamoin. Nn-mcre: a modified constitutive relation error framework for unsupervised learning of nonlinear state laws with physics-augmented neural networks. 2023.
- [23] Qiang Yang, Yu Zhang, Wenyuan Dai, and Sinno Jialin Pan. *Transfer learning*. Cambridge University Press, 2020.
- [24] Digimat-MF. <https://www.e-xstream.com/products/digimat/tools?MF=1>. Accessed: October 2, 2016.
- [25] Johannes Dornheim, Lukas Morand, and Dirk Helm. Neural networks for constitutive modeling—from universal function approximators to advanced models and the integration of physics. *arXiv preprint arXiv:2302.14397*, 2023.
- [26] Razvan Pascanu, Tomas Mikolov, and Yoshua Bengio. On the difficulty of training recurrent neural networks. In *International conference on machine learning*, pages 1310–1318. Pmlr, 2013.
- [27] Diab W Abueidda, Seid Koric, Nahil A Sobh, and Huseyin Sehitoglu. Deep learning for plasticity and thermo-viscoplasticity. *International Journal of Plasticity*, 136:102852, 2021.
- [28] Dengpeng Huang, Jan Niklas Fuhg, Christian Weißenfels, and Peter Wriggers. A machine learning based plasticity model using proper orthogonal decomposition. *Computer Methods in Applied Mechanics and Engineering*, 365:113008, 2020.

- [29] Nikolaos N Vlassis and WaiChing Sun. Geometric learning for computational mechanics part ii: Graph embedding for interpretable multiscale plasticity. *Computer Methods in Applied Mechanics and Engineering*, 404:115768, 2023.
- [30] Reese E Jones, Ari L Frankel, and KL Johnson. A neural ordinary differential equation framework for modeling inelastic stress response via internal state variables. *Journal of Machine Learning for Modeling and Computing*, 3(3), 2022.
- [31] I. Doghri and L. Tinel. Micromechanical modeling and computation of elasto-plastic materials reinforced with distributed-orientation fibers. *Int. J. Plast.*, 21(10):1919–1940, October 2005.
- [32] SM Mirkhalaf, FM Andrade Pires, and R Simoes. An elasto-viscoplastic constitutive model for polymers at finite strains: Formulation and computational aspects. *Computers & Structures*, 166:60–74, 2016.
- [33] SM Mirkhalaf, FM Andrade Pires, and Ricardo Simoes. Modelling of the post yield response of amorphous polymers under different stress states. *International Journal of Plasticity*, 88:159–187, 2017.
- [34] Juan C Simo and Thomas JR Hughes. *Computational inelasticity*, volume 7. Springer Science & Business Media, 2006.
- [35] Christopher M Bishop and Nasser M Nasrabadi. *Pattern recognition and machine learning*, volume 4. Springer, 2006.
- [36] Andrea Saltelli, Paola Annoni, Ivano Azzini, Francesca Campolongo, Marco Ratto, and Stefano Tarantola. Variance based sensitivity analysis of model output. design and estimator for the total sensitivity index. *Computer Physics Communications*, 181(2):259–270, 2010.
- [37] Marissa Renardy, Louis R. Joslyn, Jess A. Millar, and Denise E. Kirschner. To sobol or not to sobol? the effects of sampling schemes in systems biology applications. *Mathematical Biosciences*, 337:108593, 2021.
- [38] Laurens van der Maaten and Geoffrey Hinton. Visualizing data using t-sne. *Journal of Machine Learning Research*, 9(86):2579–2605, 2008.
- [39] Geoffrey E Hinton and Sam Roweis. Stochastic neighbor embedding. *Advances in neural information processing systems*, 15, 2002.
- [40] Bernhard Mehlig. *Machine Learning with Neural Networks: An Introduction for Scientists and Engineers*. Cambridge University Press, 1 edition, 2021.

- [41] Julian N Heidenreich, Colin Bonatti, and Dirk Mohr. Transfer learning of recurrent neural network-based plasticity models. *International Journal for Numerical Methods in Engineering*, 2023.
- [42] William Chan, Navdeep Jaitly, Quoc V Le, and Oriol Vinyals. Listen, attend and spell. *arXiv preprint arXiv:1508.01211*, 2015.
- [43] Ilya Sutskever, Oriol Vinyals, and Quoc V Le. Sequence to sequence learning with neural networks. *Advances in neural information processing systems*, 27, 2014.
- [44] Jack S Callaghan, Duncan Crump, Anette S Nielsen, OT Thomsen, and Janice M Dulieu-Barton. Quantitative full-field data fusion for evaluation of complex structures. *Experimental Mechanics*, pages 1–21, 2023.
- [45] Jiyoung Jung, Yongtae Kim, Jinkyoo Park, and Seunghwa Ryu. Transfer learning for enhancing the homogenization-theory-based prediction of elasto-plastic response of particle/short fiber-reinforced composites. *Composite Structures*, 285:115210, 2022.
- [46] Zachary C Lipton, John Berkowitz, and Charles Elkan. A critical review of recurrent neural networks for sequence learning. *arXiv preprint arXiv:1506.00019*, 2015.
- [47] Junyoung Chung, Caglar Gulcehre, KyungHyun Cho, and Yoshua Bengio. Empirical evaluation of gated recurrent neural networks on sequence modeling. *arXiv preprint arXiv:1412.3555*, 2014.
- [48] Kyunghyun Cho, Bart Van Merriënboer, Dzmitry Bahdanau, and Yoshua Bengio. On the properties of neural machine translation: Encoder-decoder approaches. *arXiv preprint arXiv:1409.1259*, 2014.
- [49] Author(s) of the Documentation. The mathworks, inc. deep learning toolbox: User’s guide. MATLAB Documentation, 2021.
- [50] Aurélien Géron. *Hands-on machine learning with Scikit-Learn, Keras, and TensorFlow.* ” O’Reilly Media, Inc.”, 2022.
- [51] Cort J Willmott and Kenji Matsuura. Advantages of the mean absolute error (mae) over the root mean square error (rmse) in assessing average model performance. *Climate research*, 30(1):79–82, 2005.
- [52] C3SE - About Vera. <https://www.c3se.chalmers.se/documentation/intro-vera/slides/>. Accessed on June 2, 2023.

- [53] Diederik P Kingma and Jimmy Ba. Adam: A method for stochastic optimization. *arXiv preprint arXiv:1412.6980*, 2014.
- [54] Nitish Srivastava, Geoffrey Hinton, Alex Krizhevsky, Ilya Sutskever, and Ruslan Salakhutdinov. Dropout: A simple way to prevent neural networks from overfitting. *Journal of Machine Learning Research*, 15(56):1929–1958, 2014.
- [55] Kevin P Murphy. *Machine learning: a probabilistic perspective*. MIT press, 2012.